Design of Double-Passed Arrayed-Waveguide Gratings for the Generation of Flat-Topped Femtosecond Pulse Trains

Bhaskaran Muralidharan, Venkataramanan Balakrishnan, *Member, IEEE*, and Andrew M. Weiner, *Fellow, IEEE*

***Abstract*—This paper presents a theoretical investigation of femtosecond flat-topped pulse-sequence generation using an arrayed-waveguide grating (AWG) in a double-passed configuration. We present low-insertion-loss designs using phase-only filters designed using numerical optimization. The designs are also analyzed for robustness to fabrication errors.**

***Index Terms*—Arrayed-waveguide grating (AWG), optical pulse generation, phase-only filter, wavelength-division multiplexing (WDM).**

I. Introduction

THE arrayed-waveguide grating (AWG) is now a well-known technology that is deployed for applications in wavelength-division-multiplexed (WDM) channel demultiplexers and optical routers [1]–[6]. A few recent experiments [7]–[10] have demonstrated a completely new functionality of the AWG. In the initial experiment by Leaird *et al.* [7], the AWG was read out by a femtosecond pulse to yield a burst consisting of tens of femtosecond pulses under a Gaussian envelope. The pulse-repetition rate is set by the delay increment in the waveguide-array section and can be in the several hundred gigahertz to terahertz range. A subsequent experiment introduced loss engineering (i.e., adding attenuation to appropriate waveguides in the waveguide array) to shape the pulse-train envelope to have a flat-topped (equal intensity) character [9]. By combining two outputs of such a loss-engineered AWG read out by a high-rate modelocked fiber laser, generation of a 500-GHz continuous pulse train was achieved [10]; this constituted a 42-fold repetition-rate multiplication factor compared to the 11.9-GHz rate of the modelocked laser. Another experiment that recombined multiple outputs of the AWG by using double-pass geometry showed promise for a much higher repetition-rate multiplication factors in the range of several hundreds, with the possibility of fundamentally low insertion loss [8]. However, loss engineering directly gives rise to excess insertion loss and, more fundamentally, does not appear to provide for a flat-topped intensity envelope when used in the double-pass geometry. The principal contribution of this paper is the design of AWGs that when employed in a double-passed configuration yield long pulse trains with a square envelope, yet minimizing excess insertion loss via the use of a phase-only approach. This is achieved via numerical optimization [13], using as parameters the phases of the individual waveguides that constitute the AWG. We will also demonstrate that the proposed approach allows a systematic tradeoff between the various design objectives such as the flatness of the pulse-train temporal envelope, the length of the envelope, and energy loss. Numerical simulations establish that the designs are "robust," i.e., the performance of the designs degrades gracefully in the presence of fabrication errors, thus encouraging their practical implementation.

This paper is structured as follows. In Section II, we review relevant results from the previous work on the time-domain response of the AWGs, while introducing a mathematical framework for the AWG from a systems perspective convenient for the optimization work. Section III defines our optimization approach. Section IV presents the simulation results for pulse sequences designed via our optimization approach. Simulation results testing the robustness of design waveforms are also discussed. We conclude with Section V.

We note that others have investigated AWG designs in which individual waveguide phases are manipulated, e.g., [11] and [12]. In the prior work, the focus is on the frequency-domain response of the AWG, e.g., tailoring the passband shapes or the dispersion. In contrast, in the current paper, for the first time, we investigate the design of waveguide phases such that a desired time-domain response is obtained, in particular the double-pass intensity profile.

II. Time-Domain Response of the AWG and the Mathematical Framework

We consider an AWG with light coupled in via a single input guide, with $2M+1$ waveguides in the waveguide-array section. We make the following assumptions.

1) The delay increment τ between two consecutive waveguides in the array is a constant.
2) We consider the response to an individual input pulse with pulsewidth $t_{\rm p}$ less than the delay increment per guide $t_{\rm p} < \tau$. This means that laser bandwidth exceeds the AWG's free spectral range (FSR), which is determined by the delay increment through the well-known relationship FSR $= (1/\tau)$.

Manuscript received October 16, 2004; revised August 23, 2005. This work was supported in part by the National Science Foundation under Grant ECS-0100949.

The authors are with the School of Electrical and Computer Engineering, Purdue University, West Lafayette, IN 47907-1285 USA (e-mail: bmuralid@ecn.purdue.edu; ragu@ecn.purdue.edu; amw@ecn.purdue.edu).

Digital Object Identifier 10.1109/JLT.2005.860154

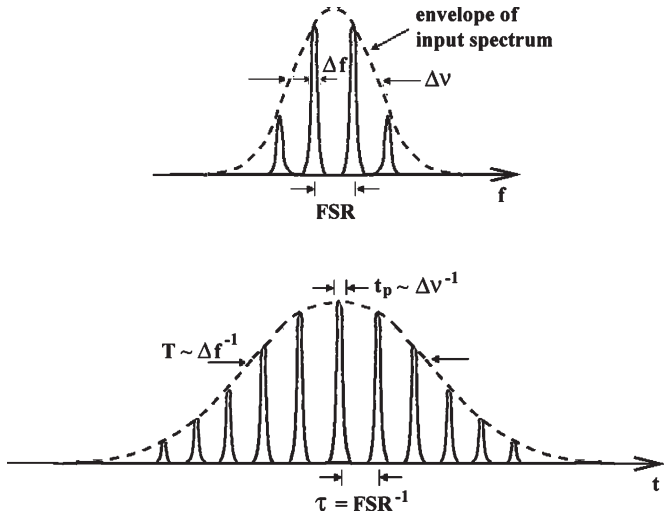

Fig. 1. Expected output spectrum and temporal profile for an arbitrary output guide of the AWG (modified from [7]). Note that an output pulse sequence is generated from every laser input pulse; only the response to a single laser pulse is depicted in the figure.

3) The dispersion in the individual waveguides in the waveguide array is negligible.

Let the input pulse be $e_{\rm in}(t)\mathrm{e}^{j\omega_{\rm c}t}$, with spectrum (Fourier transform) $E_{\rm in}(j(\omega-\omega_{\rm c}))$. With $t_{\rm p}$ denoting the input pulsewidth, and the bandwidth of $E(j\omega)$ is proportional to $1/t_{\rm p}$. Under the assumptions, at each output waveguide, the phase-match condition is satisfied for a series of frequencies spaced by the FSR, but with a slight frequency shift (less than the FSR) from one output guide to the next. Thus, the spectrum of the signal at the nth output guide of the AWG is then given by

$$E_{\rm out}^{(n)}(j\omega)=\sum_{k=-\infty}^{\infty}E_{\rm in}\left(j(\omega-\omega_{\rm c})\right)S\left(j\left(\omega-\omega_n-\frac{2\pi k}{\tau}\right)\right) \tag{1}$$

where ω_n denotes the center frequency (taken within a single diffraction order of the AWG) corresponding to the nth output waveguide, and $S(j(\omega-\omega_{\rm pm}))$ represents the bandpass characteristics of the AWG around any frequency $\omega_{\rm pm}$ where phase match occurs. This is well known from numerous studies of the AWG as a frequency-demultiplexing device. It is convenient to choose $\omega_{\rm c}=\omega_0$, i.e., $\omega_{\rm c}$ is chosen equal to a pass frequency for the central $(n=0)$ output guide. For future reference, we let $s(t)$ denote the inverse Fourier transform of $S(j\omega)$, and T denote the effective width (i.e., temporal extent) of $s(t)$. The bandwidths of $E_{\rm in}(j\omega)$ and $S(j\omega)$ are denoted $\Delta\nu$ and Δf, and are proportional to $1/t_{\rm p}$ and $1/T$, respectively. A representative plot of $E_{\rm in}(j\omega)$ and $S(j\omega)$, under the assumptions, is shown in Fig. 1. Thus, at the nth output waveguide, the AWG functions as a bank of narrow bandpass filters, centered at frequencies $\omega_n+(2\pi k/\tau)$, where k is an integer.

We next consider the temporal response at the nth output waveguide. From the inverse Fourier transform of (1)

$$e_{\rm out}^{(n)}(t)=\sum_{k=-\infty}^{\infty}\left(e_{\rm in}(t)\mathrm{e}^{j\omega_0 t}\right)\star\left(s(t)\mathrm{e}^{j\omega_n t}\mathrm{e}^{j\frac{2\pi k}{\tau}t}\right) \tag{2}$$

where "$\star$" denotes convolution. Using the identity

$$\sum_{k=-\infty}^{\infty}\mathrm{e}^{j\frac{2\pi k}{\tau}t}=\tau\sum_{k=-\infty}^{\infty}\delta(t-k\tau) \tag{3}$$

we have

$$\begin{aligned}e_{\rm out}^{(n)}(t)&=\tau\left(e_{\rm in}(t)\mathrm{e}^{j\omega_0 t}\right)\star\left(\sum_{k=-\infty}^{\infty}s(t)\mathrm{e}^{j\omega_n t}\delta(t-k\tau)\right)\\&=\tau\left(e_{\rm in}(t)\mathrm{e}^{j\omega_0 t}\right)\star\left(\sum_{k=-\infty}^{\infty}s(k\tau)\mathrm{e}^{jk\omega_n\tau}\delta(t-k\tau)\right).\end{aligned} \tag{4}$$

Note here that for our choice of $\omega_{\rm c}=\omega_0$, coinciding with the transmission peak of the central output guide, we have $\omega_0\tau=2m\pi$, which is the condition for constructive interference. Thus, from a time domain perspective, the AWG as viewed by the nth output guide behaves, in effect, as a collection of delay lines, with a delay increment of τ, a phase-shift increment of $(\omega_n-\omega_0)\tau$, and a transmission amplitude of $s(k\tau)$ for the kth delay line. As sketched in Fig. 1, for a short pulse input, the output is a sequence of pulses with pulse spacing τ. The amplitude of the kth pulse $s(k\tau)$ is physically equal to the amplitude of the field component coupled from the input guide through the kth guide in the waveguide array to the nth output guide. The $\mathrm{e}^{jk(\omega_n-\omega_0)\tau}$ term acts to pick out frequency components for the nth output guide that are shifted by $\omega_n-\omega_0$ relative to those in the central guide. Since $s(k\tau)$ is independent of output-guide number, pulse sequences with identical intensity profiles but with slight shifts in their frequency combs are produced at each of the output guides, as demonstrated in [7]. The different $s(k\tau)$ can be modified by inserting various attenuations into the different guides in the array; this is the basis for waveform control via loss engineering, as demonstrated in [9].

Consider now a small change $\Delta\tau_k$ in the delay of the kth waveguide, where $\Delta\tau_k$ is taken to be on the order of one optical cycle or less. This would physically correspond to altering the length of the kth waveguide by a small path length δL_k where δL_k is on the order of one wavelength or less. This would imply that $k\tau\rightarrow k\tau+\Delta\tau_k$. Consequently, the output will be

$$\begin{aligned}&e_{\rm out}^{(n)}(t)\\&\quad\approx\tau\left(e_{\rm in}(t)\mathrm{e}^{j\omega_0 t}\right)\\&\qquad\star\left(\sum_{k=-\infty}^{\infty}s(k\tau)\mathrm{e}^{j\omega_0(k\tau+\Delta\tau_k)}\mathrm{e}^{j(\omega_n-\omega_0)(k\tau+\Delta\tau_k)}\delta(t-k\tau)\right)\\&\quad\approx\tau(e_{\rm in}(t)\mathrm{e}^{j\omega_0 t})\\&\qquad\star\left(\sum_{k=-\infty}^{\infty}s(k\tau)\mathrm{e}^{j\omega_0\Delta\tau_k}\mathrm{e}^{jk(\omega_n-\omega_0)\tau}\delta(t-k\tau)\right)\end{aligned} \tag{5}$$

where we have used $\mathrm{e}^{j\omega_0 k\tau}=1$ and made the approximation $|(\omega_n-\omega_0)\Delta\tau_k|\ll 1$, which is valid as long as $|\omega_n-\omega_0|\ll\omega_0$.

Thus, in summary, the impulse response of the envelope from the input to the nth output guide can be modeled as

$$h^{(n)}(t) = \tau \sum_{k=-M}^{M} b_k e^{jk(\omega_n-\omega_0)\tau}\delta(t-k\tau)$$
$$= \tau \sum_{k=-M}^{M} b_k e^{j(\omega_n-\omega_0)t}\delta(t-k\tau) \quad (6)$$

where $b_k = s(k\tau)e^{j\omega_0\Delta\tau_k}$, and $b_k = 0$ for $|k| > M$ (since there are only $2M+1$ waveguides, by assumption). Through loss engineering and by changing the length of the kth waveguide, we may change the magnitude and phase, respectively, of b_k.

In the double-passed configuration, these pulse bursts observed at different output guides are recombined into a single optical channel by returning them through the AWG using a mirror and a suitable set of delays. For simplicity, we restrict our attention to the case of an AWG where the input and output slab regions are identical. Then, from symmetry, the contribution of the double-pass envelope response corresponding to the nth output waveguide is simply the autoconvolution $g^{(n)} = h^{(n)} \star h^{(n)}$. Thus, the contribution of the nth output waveguide to the double-passed response is

$$g^{(n)}(t) = \tau^2 e^{j(\omega_n-\omega_0)t}\sum_i a_i\delta(t-i\tau) \quad (7)$$

where

$$a_i = \sum_k b_k b_{i-k}. \quad (8)$$

Such autoconvolution behavior has been observed experimentally—compare measured intensity profiles in Fig. 2 for a loss-engineered device for single- and double-passed operation, respectively (reprinted from [8]). Clearly, the flat-topped intensity profile is lost upon the double passing of the device. Our design goal in this paper will be to achieve flat-topped behavior in double pass by appropriately designing the b_k in (6). In the experiment of [8], pulse trains from various output guides were recombined with delays such that the contributions from different output guides are not overlapped in time. Under this condition, the different pulse trains have identical intensity profiles and add incoherently. From the design perspective, it is then sufficient to consider the double-pass waveform contributed by a single output guide. This is the approach we will adopt in the remainder of this paper.

III. Optimization Approach

Our approach in designing waveguide phases using an optimization approach and eventually picking out optimal designs adopts the following flow as depicted in Fig. 3.

1) Begin with a verbally expressed design objective.
2) Make any necessary assumptions, and translate it into an optimization problem (this involves finding the constraints, variables, and objective).
3) Evaluate any design systematically for performance and robustness.

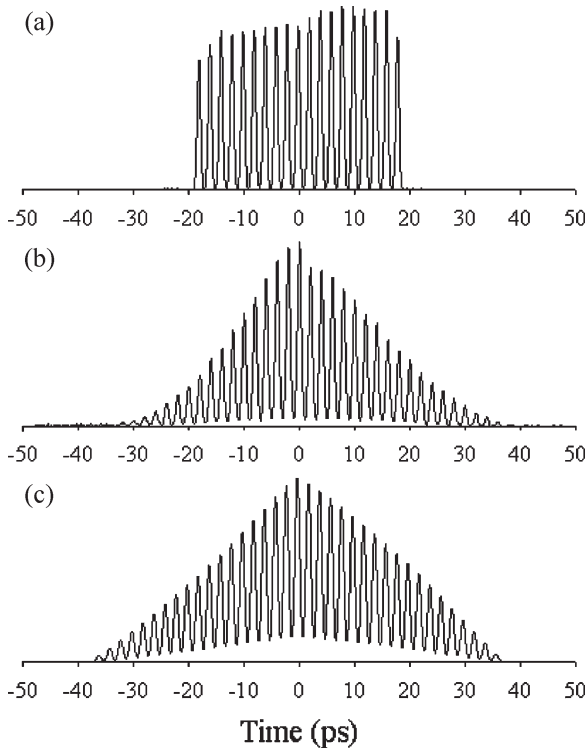

Fig. 2. Output pulse trains. (a) Single pass through the AWG. (b) Double pass. (c) Calculated output-pulse train obtained by autoconvolving the single-pass temporal response (from Leaird *et al.* [8]).

We now explore the problem of designing AWGs where a single input pulse, after a double pass, yields a train of pulses whose heights are approximately the same, i.e., "flat-topped." We will restrict our attention to the case when the output from a single output waveguide is returned through the AWG using a mirror. Our design objectives are the following.

1) The double-passed output waveform should be close to an ideal square train of pulses, i.e., with constant amplitude in the temporal region of the pulse train, and zero amplitude elsewhere.
2) The energy efficiency should be high, i.e., the energy of the double-passed output must be as close as possible to the energy of the input pulse.

We now proceed towards formally translating these design objectives into a numerical-optimization problem. Let K denote the number of desired pulses in the double-passed output. For convenience, we assume that K is odd, and let $K = 2l+1$. Without loss of generality, we assume that the output-pulse-train amplitude is normalized to unity.

A. Constraints

1) The first design objective, that the output pulse train be as close to an ideal square pulse train, yields the constraint

$$\left|\,|a_i| - 1\,\right| \le \epsilon_1, \quad -l \le i \le l$$
$$|a_i| \le \epsilon_2, \quad \text{otherwise} \quad (9)$$

where the variables a_i characterize the double-passed output via (8). The variables ϵ_1 and ϵ_2 represent the

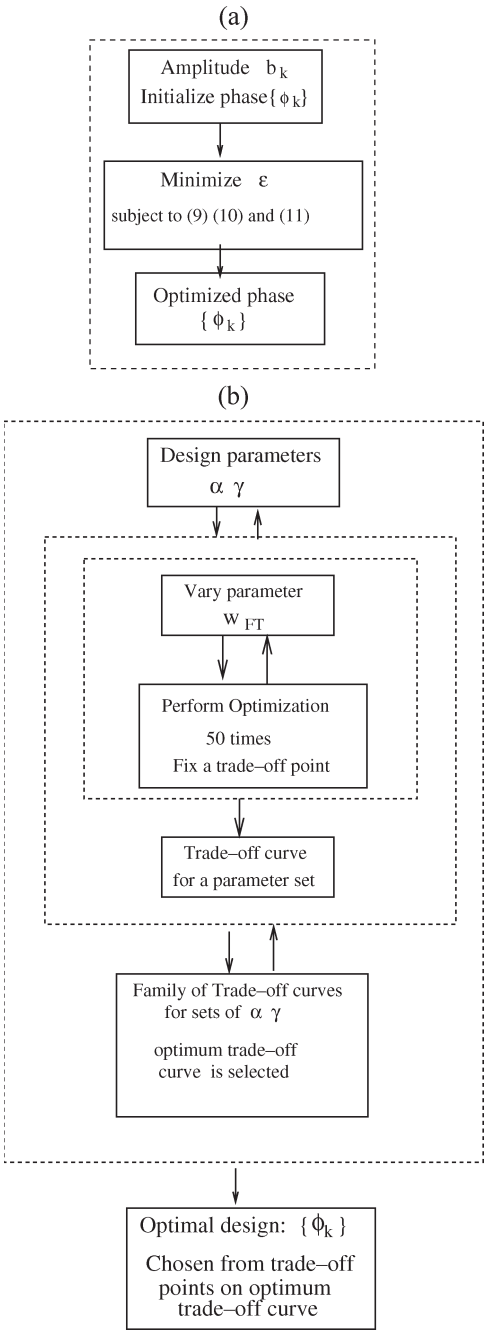

Fig. 3. Block diagram of the optimization procedure and design evaluation. (a) Optimization procedure yields the optimized set of waveguide phase ϕ_k. (b) Block diagram showing the design-evaluation process using tradeoff curves described in text. This leads to the selection of optimal designs (phase profiles) for both the 11-pulse/19-waveguide and 19-pulse/39-waveguide systems.

deviation from the ideality of the output pulse train in the temporal region of the pulse train and outside (henceforth referred to as the "wings"), respectively. A smaller value of ϵ_1 ensures a flatter pulse train, while a smaller value of ϵ_2 ensures that the pulse train cuts off sharply.

2) The second design objective, that the transmission losses be low, is handled indirectly in the spectral domain. Rather than directly address the insertion loss, we connect the insertion loss with the shape of the double-passed transfer-function magnitude, which exhibits a strong peak at frequencies $\omega_n + (2\pi k/\tau)$. Intuition suggests that the excess insertion loss may be minimized by peaking the spectral energy around these frequencies. A formulation for computing the excess insertion loss will be discussed later. However, for a standard AWG, it is well known that the wavelengths demultiplexed in one AWG can be recombined by passing through an identical second AWG (or double passing back through the first AWG). Therefore, in order to minimize excess loss in the modified AWGs we wish to design, one should seek to retain the strongly peaked spectral character of the standard AWG. We implement this idea in our optimization problem by defining a small band called the "in-band" around the peak frequencies. We take α as the ratio of the energies contained outside and inside the in-band. Then, the spectral peaking constraint, which is an indirect enforcement of the insertion-loss constraint, can be formulated as

$$\int_{\text{out-band}} |H(j\omega)|^2 \, d\omega \le \alpha \int_{\text{in-band}} |H(j\omega)|^2 \, d\omega \quad (10)$$

where $H(j\omega)$ is the Fourier transform of the impulse-response function of the central output waveguide and represents its output spectral properties. The width of the in-band is arbitrarily chosen to be the 10-dB width of the Gaussian transmission of the unperturbed AWG. Other choices of the in-band width are equally effective. As α takes on smaller values, there is sharper peaking of energy inside the in-band, leading to a decrease in the excess insertion loss.

B. Optimization Variables

Recall that our design freedom is the ability to change the magnitude of b_k through loss engineering, and their phase through changing the corresponding waveguide lengths [see (6)]. Loss engineering, in light of the interpretation of the AWG as comprising a collection of delay lines, provides a direct way of achieving flat-topped-pulse-train output when the AWG is used in single pass. However, in this paper, we are concerned with the generation of flat-topped pulse trains using the AWG in double pass. In this double-pass case, loss engineering alone does not appear to be capable of producing a flat-topped pulse train, due to the autoconvolution effect illustrated in Fig. 2. Therefore, manipulation of phase appears necessary. In principle, it is possible to use both amplitude and phase as design parameters. However, since tailoring with the amplitude inevitably adds insertion loss, we take the approach of regarding only the phases of b_k as design variables; the magnitudes of b_k are considered to be constant and are set, from the physics of propagation through the free propagation region (FPR), to be approximately Gaussian, with the central waveguide collecting the maximum energy. Thus, we have

$$|b_n| = b_0 \mathrm{e}^{\frac{-n^2}{\gamma^2}}, \quad n = -M, -(M-1), \ldots, M-1, M \quad (11)$$

where γ is a device parameter that controls the width of the Gaussian profile. Physically, γ can be adjusted, for example,

by changing the center-to-center spacing of the guides in the waveguide array, while keeping the rest of the AWG design constant. Writing $b_n = |b_n|e^{j\phi_n}$, the optimization variables are thus the phase terms ϕ_n.

C. Optimization Problem

Recall that ϵ_1 and ϵ_2 control the deviation of the output pulse train from the ideal square train. We take $\epsilon_1 = w_{\rm FT}\epsilon$, and $\epsilon_2 = w_{\rm WI}\epsilon$, so as to have a single variable ϵ; the parameters $w_{\rm FT}$ and $w_{\rm WI}$ reflect the relative weights that we assign between the desired properties of pulse train flatness and sharp cutoff of the pulse train wings. Then, we fix the values of

1) K, the desired number of pulses in the double-passed output;
2) the parameter α that controls the ratio of the out-of-band to in-band energy [see (10)];
3) the parameter γ that characterizes the shape of the Gaussian profile of the magnitude of b_k [see (11)];
4) the parameters $w_{\rm FT}$ and $w_{\rm WI}$ that determine ϵ_1 and ϵ_2 in (9), thus characterizing the tradeoff between pulse-train flatness and cutoff.

and solve the optimization problem

$$\begin{aligned} &\text{minimize} : \epsilon \\ &\text{subject to} : (9), (10), \text{ and } (11). \end{aligned} \tag{12}$$

Given a set of design parameters K, α, and γ, we calculate the optimal phase values via numerical optimization, as shown in the block diagram in Fig. 3(a).

D. Design Evaluation

By numerically solving a series of optimization problems (12) for various values of K, α, γ, $w_{\rm FT}$, and $w_{\rm WI}$, we may systematically explore the interplay between the various parameters that affect the constraints. This in turn enables us to study the tradeoff between the conflicting objectives of squareness of the output pulse train and low insertion loss.

The following quantitative measures will be used to evaluate the designs obtained.

1) How close the output pulse train is to the ideal square train is captured by the quantities $\delta_{\rm FT}$ and $\delta_{\rm WI}$, defined as

$$\delta_{\rm FT} = \max_{l \le i \le l} \big|\, |a_i|^2 - 1 \,\big|, \quad \delta_{\rm WI} = \max_{l > |i|} |a_i|^2. \tag{13}$$

   $\delta_{\rm FT}$ serves to quantify how flat-topped the output pulse train is, and $\delta_{\rm WI}$ measures the electric-field intensity in the wings, i.e., it quantifies how sharply the pulse train cuts off.
2) The insertion loss is computed as follows. The single-pass impulse response $h^{(n)}$ is given by (6), with transfer function

$$H^{(n)}(j\omega) = \tau \sum_{k=-M}^{M} b_k e^{jk(\omega_n - \omega_0)\tau} e^{-jk\omega\tau}. \tag{14}$$

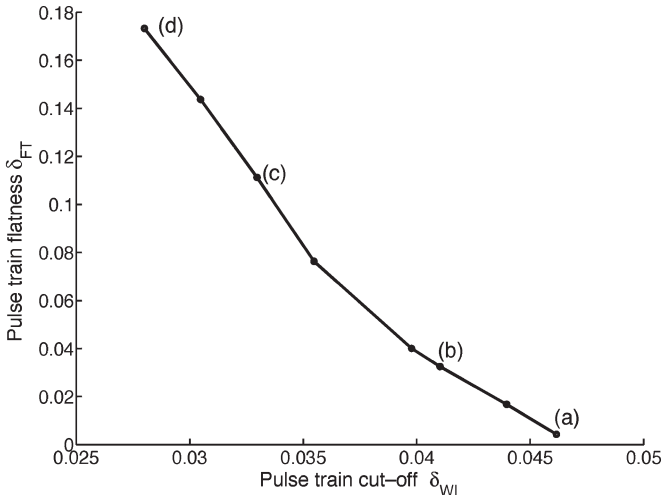

Fig. 4. Sample tradeoff curve. Here, we have set $\gamma = 0.83M$ and $\alpha = 0.45$. We obtain the various points by setting $w_{\rm WI} = 1$ and varying $w_{\rm FT}$ gradually. Points marked (a) through (d) correspond to $w_{\rm FT} = 0.01, 0.04, 0.4,$ and 0.7, respectively.

Specializing to the central output guide ($\omega_n = \omega_0$), which is sufficient for our purposes, we have

$$H^{(0)}(j\omega) = \tau \sum_{k=-M}^{M} b_k e^{-jk\omega\tau}. \tag{15}$$

We will henceforth simplify our notation by writing $H(j\omega)$ instead of $H^{(0)}(j\omega)$; the implication is that we are specializing to the central output guide, although as discussed earlier, all of the output guides give very similar responses. The double-pass impulse response is given by the convolution $g^{(n)} = h^{(n)} \star h^{(n)}$, and consequently the double-pass transfer function is $G(j\omega) = H^2(j\omega)$. Note that $H(j\omega)$ and $G(j\omega)$ are periodic in ω. With the assumption that the input spectrum is broad (i.e., the input pulse can be well approximated by an impulse function), the power from one output waveguide double passed through the AWG is simply proportional to

$$P_{\rm d} = \int_{-\frac{\pi}{\tau}}^{\frac{\pi}{\tau}} |H(j\omega)|^4 \, d\omega. \tag{16}$$

Here, we have calculated only the power in one period of $H(j\omega)$; for a broad flat input spectrum, the total power is just the power per period times the number of periods excited by the input pulse. Also, as explained earlier, we assume that if multiple outputs are double passed through the AWG, then their relative delays are sufficient that there can be no temporal overlap. This ensures that the power contributions from each of them can be added, so that (16) gives the double-passed power transmission per frequency per output guide. Consequently, we can

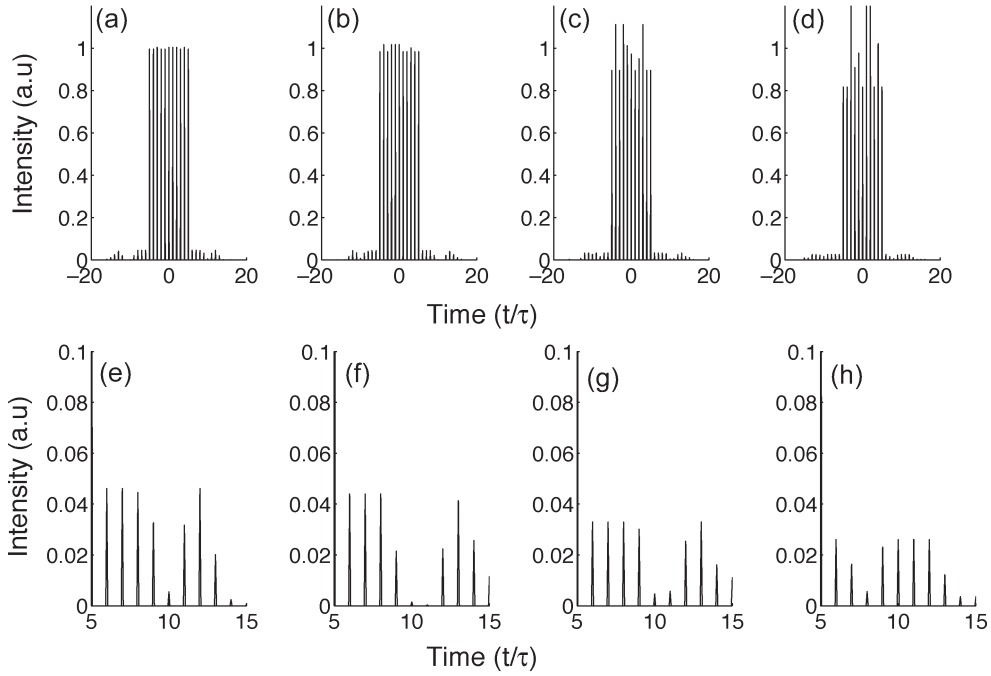

Fig. 5. Output-temporal-intensity profiles corresponding to points (a)–(d) on the tradeoff curve. (e)–(h) represent a closer look at the wing intensity corresponding to (a)–(d), respectively.

quantify the excess insertion loss with respect to the standard AWG device in decibels as

$$I_{\text{loss}} = 10\left(\log \int_{-\frac{\pi}{\tau}}^{\frac{\pi}{\tau}} |H(j\omega)|^4 d\omega - \log \int_{-\frac{\pi}{\tau}}^{\frac{\pi}{\tau}} |H_0(j\omega)|^4 d\omega\right) \tag{17}$$

where $H_0(j\omega)$ is the output passband spectrum of the untruncated AWG device (infinite number of guides in the array section) with the same excitation profile but with no added phases.

IV. Simulation Results

We solve a series of optimization problems (12), using the standard local nonlinear optimization algorithm implemented in the MatLab optimization toolbox [14], [15], with the following choices of parameters.

1) We consider two representative values for the number of output pulses: $K = 11$ and $K = 19$. This is consistent with earlier experiments [7]–[9] that typically dealt with the generation of 15 to 25 pulses per output waveguide. The corresponding number of waveguides in the AWG were chosen to be $2M + 1 = 19$ and $2M + 1 = 39$, respectively. These choices are also motivated by experiments [7], [9] that typically employed 20 or more waveguides.
2) We consider three possible choices for the parameter γ that controls the Gaussian profile of the magnitude of b_k (i.e., the excitation profile): $\gamma = 0.7M, 0.83M, M$. γ is a typical device parameter, which is controlled through the design of the splitter region of the AWG. In our case, a higher value of γ corresponds to truncating/blocking a larger number of waveguides within the intensity profile incident on the array.
3) We consider four values for the parameter α that controls the ratio of the out-of-band to in-band energy [see (10)]: $\alpha = 0.15, 0.25, 0.35, 0.45$. The use of α is proposed in order to formulate the excess-insertion-loss constraint. Choice of the above four values is followed by several trials, and depicts consistent tradeoff between spectral and temporal properties, while increasing α beyond the value of 0.45 neither illustrates any trend better nor yields better results.
4) We consider a range of values for the parameters w_{FT} and w_{WI} that reflect the relative weights that we assign between pulse-train flatness and pulse-train cutoff. The choice of parameter ranges for w_{FT} and w_{WI} was based on a subjective assessment of the obtained temporal profiles via an examination of the corresponding values of δ_{FT} and δ_{WI}.

For every parameter combination, the solution to the optimization problem (12) yields a locally optimal design, that is, a set of values for the phases ϕ_k (or in turn, a corresponding set of values of waveguide-path-length variations) that minimizes a measure of the deviation of the output pulse train from the ideal square pulse train. Owing to the "local" nature of the optimization, different runs of the optimization program with different choices of initialization of the optimization variables would yield different "optimal" solutions. To address this issue, we run the same optimization program with 50 randomly chosen initial conditions and pick the best solution, which serves as an approximation to the "globally" optimal solution.

It is impossible to present the results obtained by simultaneously varying all the parameters that characterize problem (12).

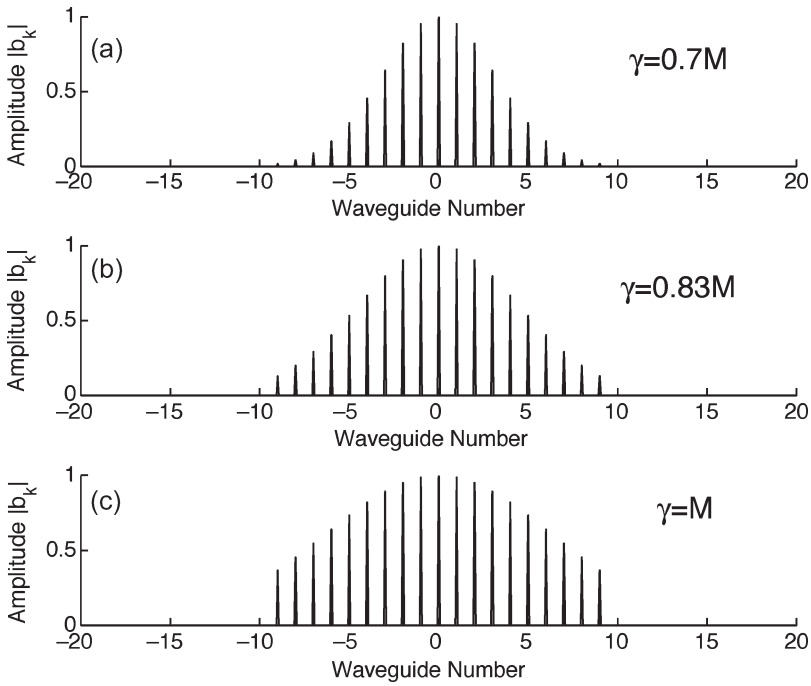

Fig. 6. Excitation profile $|b_k|$ for (a) $\gamma = 0.7M$, (b) $\gamma = 0.83M$, and (c) $\gamma = M$ for the 19-waveguide system.

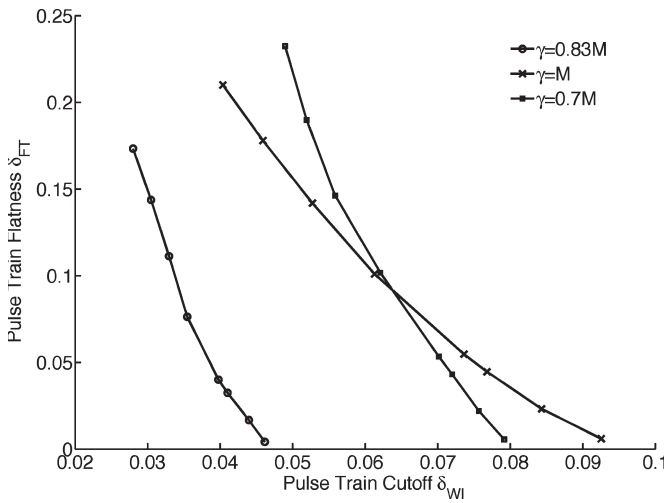

Fig. 7. Tradeoff curve for (a) $\gamma = 0.7M$, (b) $\gamma = 0.83M$, (c) $\gamma = M$ for the 11-pulse/19-waveguide system with $\alpha = 0.45$.

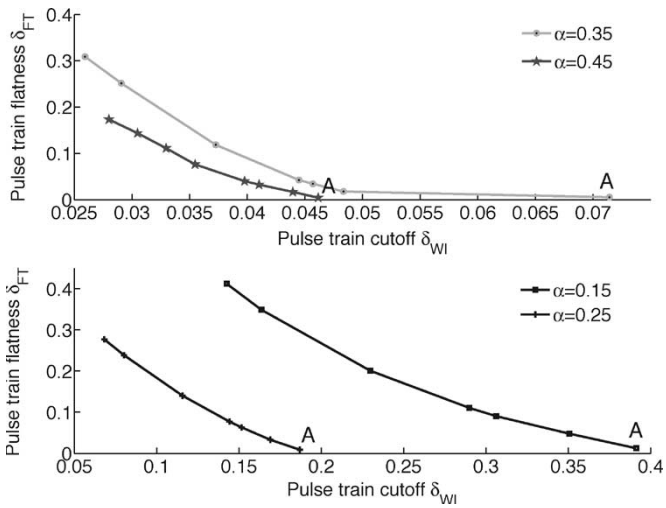

Fig. 8. Tradeoff curves for different values of α for the 11-pulse/19-waveguide system with $\gamma = 0.83M$. Points marked (A) represent the best design (by visual inspection) given any tradeoff curve due to its minimum δ_{FT}.

We instead present a series of plots, henceforth referred to as tradeoff curves, that present the performance of the optimal designs obtained by holding a subset of the parameters at a constant value and varying the remaining parameters [16]. More specifically, we hold γ and α constant, and by varying the weight parameters w_{FT} and w_{WI} systematically, obtain a series of optimal designs by numerically solving (12). The values of δ_{FT} and δ_{WI} are then plotted for the optimal designs, capturing the tradeoff between the conflicting design requirements of pulse-train flatness and pulse-train cutoff.

From the definition of the δ_{FT} and δ_{WI} in (13), it is desirable to have small values for both δ_{FT} and δ_{WI}. Thus, given a choice of two values for a parameter, say γ, the one for which the tradeoff curve is closer to the origin represents a better choice. Using this guideline, we pick one choice for both of the other parameters α and γ, and from an examination of the resulting tradeoff curve, choose one optimal design that yields reasonable values of δ_{FT} and δ_{WI}. This particular design is further analyzed for its time-domain performance. As we have noted a similar trend in the tradeoff curves for both the 19-waveguide/11-pulse and 39-waveguide/19-pulse problems, we present tradeoff curves for only the former problem. We however present the time-domain performance, designs (phases), and insertion-loss trend for two best designs from each problem. The selection process for the best designs of the latter problem follows exactly the same trend (with the same values of the variable parameters α and γ) as the former problem. The block diagram in Fig. 3(b)

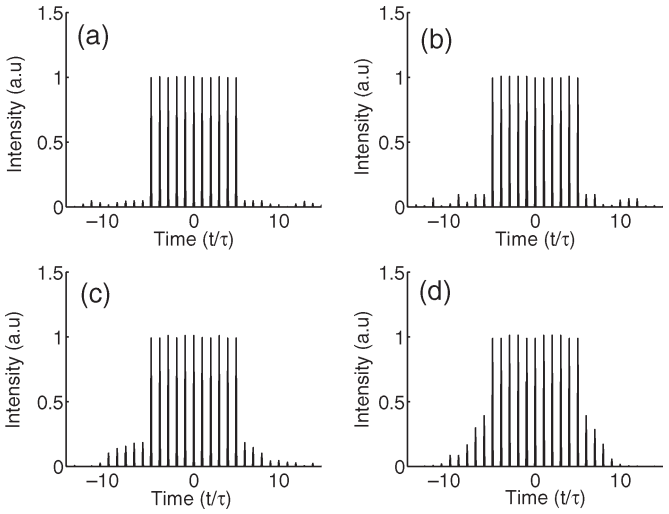

Fig. 9. Output temporal profiles corresponding to points marked (A) (representing designs with the flattest tops) on the tradeoff curves in Fig. 8 for (a) $\alpha = 0.45$; (b) $\alpha = 0.35$; (c) $\alpha = 0.25$; and (d) $\alpha = 0.15$.

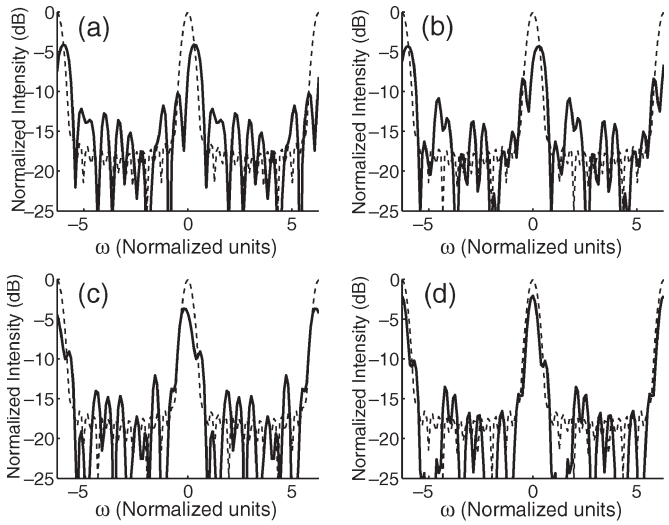

Fig. 10. Examples of normalized single-pass spectral profiles $(\log(|H(j\omega)|^2/|H_0(j\omega_0)^2|))$ for various values of α. (a) $\alpha = 0.45$; (b) $\alpha = 0.35$; (c) $\alpha = 0.25$; and (d) $\alpha = 0.15$, along with the unperturbed spectrum, corresponding to the time-domain plots from Fig. 10.

summarizes the procedure for generating tradeoff curves, following which acceptable designs may be selected.

An important practical issue is that of robustness: How gracefully does the performance of the optimal design degrade in the presence of variations in the optimization variables, i.e., the phase ϕ_k of b_k? We address this issue by allowing for random variation in ϕ_k around the optimal value, and analyze the performance of the resulting designs.

A. Sample Tradeoff Curve

We begin by presenting a typical tradeoff curve, i.e., a plot of δ_{WI} versus δ_{FT} for a fixed choice of parameters α and γ, in Fig. 4 for the 11-pulse/19-waveguide system. Fig. 5 shows the output pulse trains corresponding to the selected points marked on the tradeoff curve in Fig. 4. Points along the tradeoff curve are obtained by systematically varying the weights w_{FT} and

TABLE I
TABLE OF RANGE OF CALCULATED EXCESS INSERTION LOSS FOR DESIGNS WITH THE FLATTEST TOP (POINTS MARKED (A) ON ALL TRADEOFF CURVES SHOWN IN FIG. 8(a) AND (b) FOR VARIOUS VALUES OF α FOR THE 11-PULSE/19-WAVEGUIDE SYSTEM

α	Excess Insertion Loss (dB)
0.15	0.87 to 1.05 dB
0.25	1.97 to 2.21 dB
0.35	3.28 to 3.57 dB
0.45	4.83 to 5.12 dB

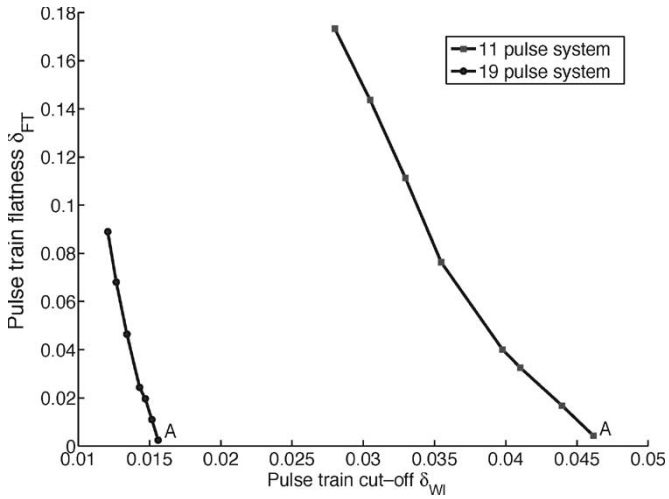

Fig. 11. Optimum tradeoff curves for 39-waveguide/19-pulse and 19-waveguide/11-pulse systems. The point marked (A) on both curves correspond to optimal designs (i.e., $\gamma = 0.83M$ and $\alpha = 0.45$).

w_{WI} as discussed earlier. We have set $w_{\mathrm{WI}} = 1$ and varied w_{FT} from 0.7 [point (d) on the tradeoff curve] to 0.01 [point (a) on the tradeoff curve]. We have used the same set of weights for all the tradeoff curves that are discussed in this paper. Notice the relative variation of pulse flatness δ_{FT} between design (d) and design (a), corresponding to the extreme points of the curve. It can be seen that the pulse-train cutoff δ_{WI} varies only by a small margin (of 2%), with δ_{FT} varying between 0.5% to 17% between the two points. Thus, a small sacrifice in δ_{WI} can be traded off to realize a large reduction in δ_{FT}.

B. Effect of γ

Recall that the parameter γ characterizes the shape of the Gaussian profile of the magnitude of b_k [see (11)]. We fix $\alpha = 0.45$ (more on this shortly), and consider three values of $\gamma : \gamma = 0.7M, 0.83M,$ and M. Recall that we have chosen an odd number of waveguides numbered from $-M$ to M. Fig. 7 illustrates the tradeoff curve between δ_{FT} and δ_{WI} for the 11-pulse/19-waveguide example $(M = 9)$. It is evident that the choice of $\gamma = 0.83M$ yields the best performance (i.e., the tradeoff curve is closest to the origin). Fig. 6 shows the magnitude profile of the coefficients b_k for the three values of γ. The double-passed output envelope is directly affected by the b_k (via an autoconvolution); this explains why γ has a significant impact on δ_{FT} and δ_{WI}. Note that our definition of γ is with respect to (11) as a fraction of the number of waveguides

TABLE II
PHASE VERSUS WAVEGUIDE NUMBER FOR TWO OPTIMAL DESIGNS FOR THE 11-PULSE/19-WAVEGUIDE SYSTEM

Waveguide number	-9	-8	-7	-6	-5	-4	-3	-2	-1	0
Phase (rad) (Design 1)	-1.3927	-0.3811	0.3378	1.5519	1.9063	1.8162	-0.0104	1.3155	0.0794	-0.6472
Phase (rad) (Design 2)	1.3587	0.8710	2.6465	0.3202	-0.7121	-1.3126	-0.3121	0.6825	1.7313	1.6703

Waveguide number	1	2	3	4	5	6	7	8	9
Phase (rad) (Design 1)	-0.7715	-0.3234	-0.0312	-0.1849	-0.8111	-1.9700	2.5555	0.0999	1.9277
Phase (rad) (Design 1)	0.9676	2.0144	1.5009	2.0087	0.3432	0.3622	-2.5299	-1.9733	-0.7468

TABLE III
PHASE VERSUS WAVEGUIDE NUMBER FOR TWO OPTIMAL DESIGNS FOR THE 19-PULSE/39-WAVEGUIDE SYSTEM

Waveguide number	-19	-18	-17	-16	-15	-14	-13	-12	-11	-10
Phase (rad) (Design 1)	1.2374	2.6319	1.6258	1.6838	0.3552	0.0732	-0.8981	-0.5698	-0.6246	2.6777
Phase (rad) (Design 2)	0.1743	1.9003	1.8631	1.4263	-0.6353	-0.5443	0.5465	-1.1562	-0.4325	2.8728

Waveguide number	-9	-8	-7	-6	-5	-4	-3	-2	-1	0
Phase (rad) (Design 1)	-2.8338	-1.2577	-0.4392	-1.7758	0.0402	-0.9946	0.1441	-0.0576	-0.0434	0.9997
Phase (rad) (Design 2)	-2.9179	-0.9400	-1.1930	0.2965	-0.9942	0.1317	-0.3099	0.5422	0.4349	1.2946

Waveguide number	1	2	3	4	5	6	7	8	9	10
Phase (rad) (Design 1)	1.7070	1.0545	0.7736	0.6322	0.7855	0.5880	0.1880	-0.5094	-2.1038	2.8506
Phase (rad) (Design 2)	2.4359	1.4315	1.3115	1.7384	1.0463	1.3376	0.8171	0.6059	3.0852	-2.5429

Waveguide number	11	12	13	14	15	16	17	18	19
Phase (rad) (Design 1)	2.3541	-1.0519	-3.0558	0.2634	-1.8500	1.0681	-1.3479	0.1871	1.0214
Phase (rad) (Design 2)	2.9206	-1.7799	-0.9385	-0.0872	1.4768	-1.1989	2.8387	1.5080	1.9950

M on each side with respect to the central waveguide. This would imply that as γ increases, we observe an increase in the amount of truncation in the Gaussian profile as seen in Fig. 6. In our formalism for the excess-insertion-loss calculation (17), we have defined $H_0(j\omega)$ as the transmission of the untruncated AWG with the same width parameter γ and with no phase perturbation. This would imply that our formalism accounts for the insertion loss due to two factors, namely 1) due to truncation of the Gaussian excitation profile and 2) due to the degradation of the lineshape arising from the phase perturbations that serve as degrees of freedom for our design problem.

C. Effect of α

Recall that the parameter α indirectly enforces the low-insertion-loss requirement via the spectral-peaking constraint (10). Fixing $\gamma = 0.83M$ (this is the best choice among the three values considered in Fig. 7), we choose four values for α: 0.15, 0.25, 0.35, and 0.45, and plot the corresponding tradeoff curves in Fig. 8(a) and (b). A smaller value of α enforces tighter spectral peaking (and a lower insertion loss) at the cost of larger deviation of the double-passed output-pulse-train envelope from the idea square train. Figs. 9 and 10 show, respectively, the output-pulse-train envelope and the normalized frequency spectrum of one optimal design for each value of α. It is evident that $\alpha = 0.15$ yields the most tightly peaked frequency spectrum, however, with the time-domain

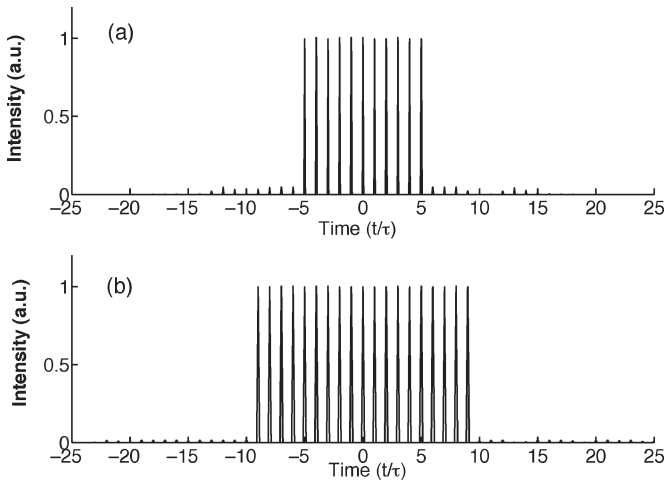

Fig. 12. Output-temporal-intensity profiles corresponding to optimum designs [corresponding to points marked (A) in Fig. 11] for 11- and 19-output pulses systems, respectively. For generating the time-domain plots, we have used design 1 from Tables II and III.

pulse envelope deviating the most from the ideal square [note that the pulse-train cutoff δ_{WI} for $\alpha = 0.45$ in Fig. 8(a) is an order of magnitude smaller than that of $\alpha = 0.15$ in Fig. 8(b)]. This would imply that an optimal design based on our analysis would be one representing point (A) on the tradeoff curve with $\alpha = 0.45$, $\gamma = 0.83M$. Designs corresponding to a particular point $(\delta_{\mathrm{WI}}, \delta_{\mathrm{FT}})$ are not unique. There can be different designs

TABLE IV
SUMMARY OF PERFORMANCE OF OPTIMAL DESIGNS (DESIGNS 1 AND 2 FROM TABLES II AND III) FOR 11-PULSE/19-WAVEGUIDE AND 19-PULSE/39-WAVEGUIDE SYSTEMS

pulse/waveguide system	11-pulse/19-waveguide	19-pulse/39 waveguide
δ_{FT}	0.2%	0.1%
δ_{WI}	4.6%	1.6%
Excess insertion loss (dB), Design 1	4.8 dB	7.26 dB
Excess insertion loss (dB), Design 2	5.08 dB	6.9 dB

(phases) with the same temporal performance (i.e., the same point on the tradeoff curve). As a result of this, the calculated excess insertion loss varies from design to design. We have generated ten designs that correspond to the points (A) (which have the flattest tops) on Fig. 8(a) and (b), and in each case, noted the trend of excess-insertion-loss variation. We generate each design by iteratively generating the same point [point (A) in our case] on the tradeoff curve. Owing to the local nature of the optimization, we obtain an entirely different design during each iteration. Table I depicts the trend of the calculated excess insertion loss [computed via (10)] for the various values of α for the 11-pulse/19-waveguide system. It is seen from Table I that our optimal designs [point (A) on $\alpha = 0.45$, $\gamma = 0.83M$ tradeoff curve] for the 11-pulse/19-waveguide system have an excess insertion loss in the range of 4.83 to 5.12 dB. Note that as α decreases, we perform significantly better spectrally (lower excess insertion loss from Table I), and at the same time, deviating more significantly from our target waveform in the time domain.

We pointed out in the beginning of this section that we shall display the selection process of the optimum design only for the 11-pulse/19-waveguide system, and choose the design with similar parameters ($\gamma = 0.83M$ and $\alpha = 0.45$) for the 19-pulse/39-waveguide system. A similar set of design parameters yields optimum designs for the 19-pulse/39-waveguide system). Fig. 11 shows tradeoff curves for both the 11-pulse/19-waveguide and 19-pulse/39-waveguide systems (in both cases, with an optimum choice of the parameters $\gamma = 0.83M$ and $\alpha = 0.45$).

The point (A) marked on both curves represents the best design in terms of best temporal shape just by visual perception. We display these designs (phase profiles) in Tables II and III with the corresponding pulse trains (design 1 from Tables II and III) in Fig. 12. Notice (in the case of the 11-pulse/19-waveguide system) that the pulse trains are nearly flat topped with pulse-train flatness at less than 0.2% variation and a marginal intensity in the wing region (less than 4%). The 19-pulse/39-waveguide system seems to have a better performance with pulse train flatness having less than 0.2% variation and the wing region having a very marginal maximum intensity of 1.6%. We estimated the excess insertion loss for this system using our formulation (once again for designs represented by the points along the $\gamma = 0.83M$ and $\alpha = 0.45$ tradeoff curve) to be in the range of 6.9 to 7.3 dB. Notice that the insertion loss for the latter system is of the order of 2 dB more than the former. Also note that the pulse-train cutoff in both cases is very sharp. We have thus obtained satisfactory designs after evaluating the interplay between several conflicting factors with the aid of tradeoff analysis. The optimal set of phases for both systems is shown in Tables II and III. It should be reiterated that we are presenting two sample sets of optimal designs. In practice, there could be several designs that yield the same temporal performance as in Fig. 12. We also summarize the performance of the optimum designs in Table IV.

TABLE V
TABLE OF PULSE-TRAIN FLATNESS TO PULSE-TRAIN CUTOFF FOR DIFFERENT EXTENTS OF PATH-LENGTH JITTERS (WORST CASE)

δL	Percentage Deviation δ_{FT}	Percent deviation δ_{WI}
Unperturbed	0.5%	4.6%
$\pm\frac{\lambda}{100}$	0.5%	4.6%
$\pm\frac{\lambda}{50}$	2%	6%
$\pm\frac{\lambda}{25}$	4%	6%
$\pm\frac{\lambda}{16}$	15%	5.5%
$\pm\frac{\lambda}{8}$	28%	8.5%

D. Robustness

In practice, any implementation of the optimal design, i.e., waveguide-length alterations, will not be exact. Thus, there remains the issue of robustness of the optimal design. We perform an empirical analysis of the optimal 11-pulse/19-waveguide design by allowing random phase errors that are uniformly distributed over a realistic range of values. Present fabrication techniques [17], [18] permit fabrication with path-length jitters typically around a twenty-fifth of a wavelength. Theoretical attempts at analyzing the effects of jitters [19], [20] have addressed the frequency response, with major focus on minimizing crosstalk due to neighboring channels. However, our robustness analysis mainly deals with the degradation of temporal properties of the obtained flat-topped pulse train with respect to random phase errors, while channel crosstalk is not an issue. In our analysis, we perturb our designs with five ranges of path-length jitter: $\pm(\lambda/100)$, $\pm(\lambda/50)$, $\pm(\lambda/25)$, $\pm(\lambda/16)$, and $\pm(\lambda/8)$. For each range, we use a uniformly distributed random variable that is added to the design phases. The resulting degradation in performance is quantified by the pulse-flatness measure δ_{FT}. This is because δ_{WI} changes from 4.5% to 8.5%, which is very slight considering the initial value of $\delta_{\mathrm{WI}} = 0.045$. For each allowable path-length-jitter range, we determine the worst-case degradation, by running 25 trials with randomly generated path-length jitters, and picking the worst (in terms of δ_{FT}). As expected, the pulse-flatness

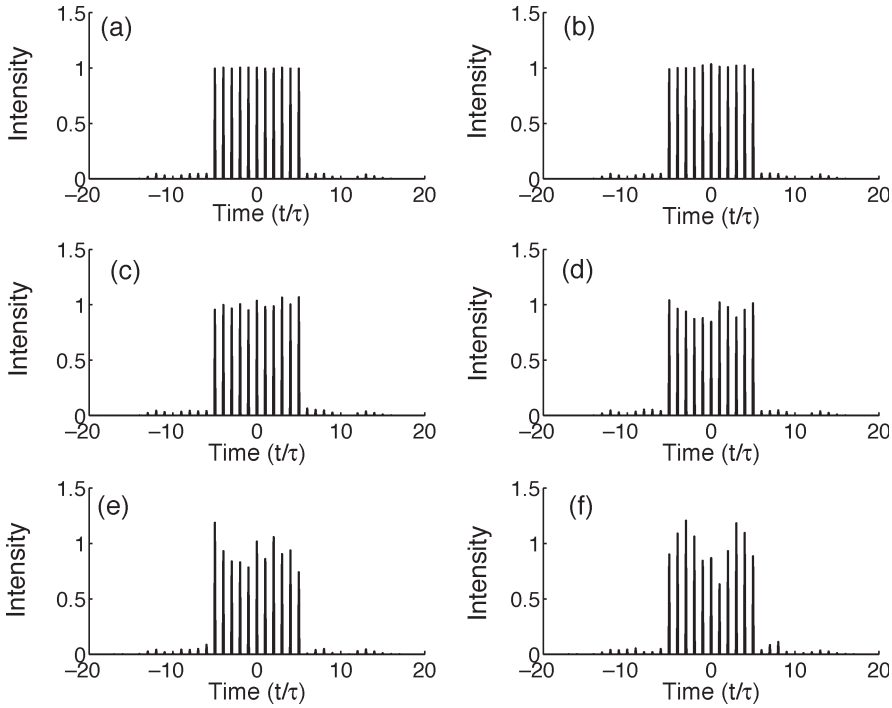

Fig. 13. Output temporal profiles for various path-length jitters for the 11-pulse system. (a) Unperturbed output. (b) $\pm(\lambda/100)$. (c) $\pm(\lambda/50)$. (d) $\pm(\lambda/25)$. (e) $\pm(\lambda/16)$. (f) $\pm(\lambda/8)$.

parameter δ_{FT} increases with the path-length-jitter range, and this variation is quite noticeable. Table V summarizes the results in comparison with the unperturbed pulse train. δ_{FT} changes from 0.5% to about 15% for a path-length-jitter range that is as high as $\pm(\lambda/16)$, and $\delta_{\mathrm{FT}} = 4\%$ in the $\pm(\lambda/25)$ range. Fig. 13 illustrates the double-pass pulse-train envelope for various path-length-jitter ranges. It turns out that the excess-insertion-loss performance degrades marginally from 4.8 dB in the unperturbed case to 4.84 dB in the worst case of $\pm(\lambda/8)$ jitter-length jitters as well; this is evident from Fig. 14, which shows the unperturbed spectrum superposed with the spectrum corresponding to the worst case degraded system due to a $\pm(\lambda/8)$ jitter. Note that with path-length jitters, the spectral shape changes only marginally, with the peaking maintained.

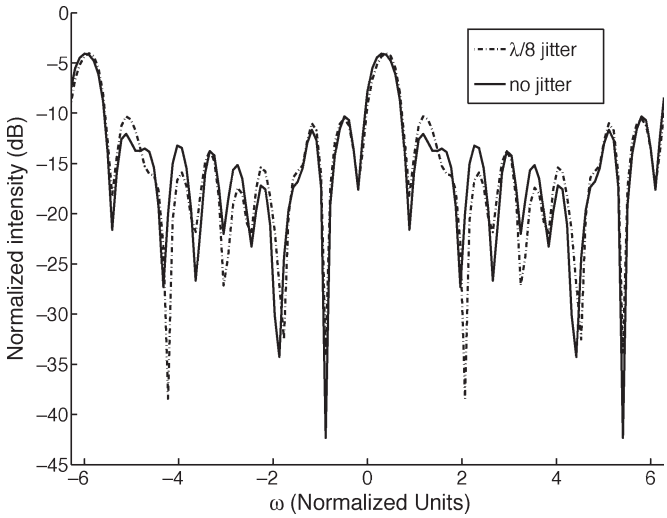

Fig. 14. Comparison of single-pass spectral profiles between the unperturbed design and with $\pm(\lambda/8)$ jitter.

V. Conclusion

We have demonstrated that by appropriately modifying the phases of the waveguides of an AWG readout by femtosecond pulses and using them in a double-passed configuration, we may generate flat-topped pulse trains with much-enhanced energy efficiency as opposed to conventional loss engineering. Moreover, the optimization framework employed offers the potential to systematically study the tradeoff between the conflicting design requirements of pulse-train flatness and pulse-train cutoff. The designs obtained appear to be robust to fabrication tolerances corresponding to phase jitter in the order of $\pm(\lambda/16)$, suggesting that the designs may be suitable for experimental implementation. As an alternative to double-passed operation, it should also be possible to cascade a pair of phase-engineered AWGs to obtain flat-topped pulse trains. Because of this, the two AWGs need not have identical designs, which would essentially double the number of optimization variables, and may lead to even better designs than the ones reported here.

References

[1] M. K. Smit, "Phasar-based WDM-devices: Principles, design and applications," *IEEE J. Sel. Topics Quantum Electron.*, vol. 2, no. 2, pp. 236–250, Jun. 1996.

[2] R. Adar, C. H. Henry, C. Dragone, R. C. Kistler, and M. A. Milbrodt, "Broad-band array multiplexers made with silica wave-guides on silicon," *J. Lightw. Technol.*, vol. 11, no. 2, pp. 212–219, Feb. 1993.

[3] H. Takahashi, K. Oda, H. Toba, and Y. Inoue, "Transmission characteristics of arrayed waveguide N by N multiplexer," *J. Lightw. Technol.*, vol. 13, no. 3, pp. 447–455, Mar. 1995.

[4] K. Okamoto, "Recent progress of integrated optics planar lightwave circuits," *Opt. Quantum Electron.*, vol. 31, no. 2, pp. 107–129, Feb. 1999.
[5] Y. Hibino, "Recent advances in high-density and large-scale AWG multi/demultiplexers with higher index contrast silica-based PLC," *IEEE J. Sel. Topics Quantum Electron.*, vol. 8, no. 6, pp. 1090–1101, Nov./Dec. 2002.
[6] J. Copmany, C. Doerr, K. Okamoto, and M. K. Smit, "Special issue on arrayed waveguide grating routers/WDM MUX/DEMUXs and related applications/uses," *IEEE J. Sel. Topics Quantum Electron.*, vol. 8, no. 6, pp. 1087–1089, Nov/Dec. 2002.
[7] D. E. Leaird, S. Shen, A. M. Weiner, A. Sugita, S. Kamei, M. Ishii, and K. Okamoto, "Generation of high repetition rate WDM pulse trains from an arrayed-waveguide grating," *IEEE Photon. Technol. Lett.*, vol. 13, no. 3, pp. 221–223, Mar. 2001.
[8] D. E. Leaird, A. M. Weiner, S. Shen, S. Kamei, M. Ishii, A. Sugita, and K. Okamoto, "Double-passed arrayed waveguide grating for 500-GHz pulse burst generation," *IEEE Photon. Technol. Lett.*, vol. 14, no. 10, pp. 1451–1453, Oct. 2002.
[9] D. E. Leaird, S. Shen, A. M. Weiner, A. Sugita, S. Kamei, M. Ishii, and K. Okamoto, "Generation of flat-topped 500-GHz pulse bursts using loss engineered arrayed waveguide gratings," *IEEE Photon. Technol. Lett.*, vol. 14, no. 6, pp. 816–818, Jun. 2002.
[10] D. S. Seo, D. E. Leaird, A. M. Weiner, S. Kamei, M. Ishii, A. Sugita, and K. Okamoto, "Continuous 500 GHz pulse train generation by repetition-rate multiplication using arrayed waveguide grating," *Electron. Lett.*, vol. 39, no. 15, pp. 1138–1140, Jul. 2003.
[11] M. C. Parker, S. D. Walker, A. Yiptong, and R. J. Mears, "Applications of active arrayed-waveguide gratings in dynamic WDM networking and routing," *J. Lightw. Technol.*, vol. 18, no. 12, pp. 1749–1756, Dec. 2000.
[12] M. C. Parker and S. D. Walker, "Design of arrayed-waveguide gratings using hybrid Fourier–Fresnel transform techniques," *IEEE J. Sel. Topics Quantum Electron.*, vol. 5, no. 5, pp. 1379–1384, Sep./Oct. 1999.
[13] V. Balakrishnan and A. Tits, "Numerical optimization-based design," in *The Control Handbook*, W. Levine, Ed. Boca Raton, FL: CRC, 1996, ch. 47, pp. 749–758.
[14] "Multiobjective optimization," *MATLAB Optimization Toolbox*, Mathworks, Natick, MA.
[15] K. Schittkowski, "NLQPL: A Fortran-subroutine solving constrained nonlinear programming problems," *Ann. Oper. Res.*, vol. 5, no. 1–4, pp. 485–500, Jun. 1985.
[16] S. Boyd and C. Barrat, *Linear Controller Design*. Englewood Cliffs, NJ: Prentice-Hall, 1991.
[17] K. Okamoto, "Tutorial: Fundamentals, technology and applications of AWG's," in *Proc. Eur. Conf. Optical Communication (ECOC)*, Madrid, Spain, Sep. 1998, pp. 35–37.
[18] T. Goh, S. Suzuki, and A. Sugita, "Estimation of waveguide phase errors in silica-based waveguides," *J. Lightw. Technol.*, vol. 15, no. 11, pp. 2107–2113, Nov. 1997.
[19] P. Munoz, D. Pastor, J. Capmany, and S. Sales, "Analytical and numerical analysis of phase and amplitude errors in the performance of arrayed waveguide gratings," *IEEE J. Sel. Topics Quantum Electron.*, vol. 8, no. 6, pp. 494–504, Dec. 2002.
[20] Y. Chu, X. Zheng, H. Zhang, X. Liu, and Y. Guo, "The impact of phase errors on arrayed waveguide gratings," *IEEE J. Sel. Topics Quantum Electron.*, vol. 8, no. 6, pp. 1122–1129, Dec. 2002.

Bhaskaran Muralidharan, photograph and biography not available at the time of publication.

Venkataramanan Balakrishnan (M'94), photograph and biography not available at the time of publication.

Andrew M. Weiner (S'84–M'84–SM'91–F'95) received the Sc.D. degree in electrical engineering from Massachusetts Institute of Technology (MIT), Cambridge, in 1984.

From 1979 through 1984, he was a Fannie and John Hertz Foundation Graduate Fellow at MIT. Upon graduation, he joined Bellcore, first as member of Technical Staff and later as Manager of Ultrafast Optics and Optical Signal Processing Research. He moved to Purdue University, West, Lafayette, IN, in 1992 and is currently the Scifres Distinguished Professor of Electrical and Computer Engineering. From 1997 to 2003, he served as the ECE Director of Graduate Admissions. His research focuses on ultrafast optical signal processing and high-speed optical communications. He is especially well known for pioneering the field of femtosecond pulse shaping, which enables generation of nearly arbitrary ultrafast optical waveforms according to user specification. He has published five book chapters and over 160 journal articles and is a coeditor of one book. He has been the author or a coauthor of over 300 conference papers, including approximately 80 conference invited talks, and has presented over 70 additional invited seminars at university, industry, and government organizations. He holds eight U.S. patents.

Prof. Weiner is a Fellow of the Optical Society of America (OSA). He has received numerous awards for his research, including the Hertz Foundation Doctoral Thesis Prize (1984), the Adolph Lomb Medal of the Optical Society of America (1990), awarded for pioneering contributions to the field of optics made before the age of 30, the Curtis McGraw Research Award of the American Society of Engineering Education (1997), the International Commission on Optics Prize (1997), the IEEE LEOS William Streifer Scientific Achievement Award (1999), the Alexander von Humboldt Foundation Research Award for Senior U.S. Scientists (2000), and the inaugural Research Excellence Award from the Schools of Engineering at Purdue (2003). He has served on or chaired numerous research review panels, professional society award committees, and conference program committees. From 1988 to 1989, he served as an IEEE Lasers and Electro-optics Society (LEOS) Distinguished Lecturer. He has served as Chair or Co-Chair of the Conference on Lasers and Electro-Optics, the Gordon Conference on Nonlinear Optics and Lasers, and the International Conference on Ultrafast Phenomena. He has also served as Associate Editor for IEEE JOURNAL OF QUANTUM ELECTRONICS, IEEE PHOTONICS TECHNOLOGY LETTERS, and *Optics Letters*. He served as an Elected Member of the Board of Governors of IEEE LEOS from 1997 to 1999 and as Secretary/Treasurer of IEEE LEOS from 2000 to 2002. From 2002 to 2005, he was a Vice-President (representing IEEE LEOS) of the International Commission on Optics (ICO).